

## Laser-induced nuclear motions in the Coulomb explosion of $C_2H_2^+$ ions

C. Cornaggia, M. Schmidt, and D. Normand

*Commissariat à l'Energie Atomique, Division des Sciences de la Matière, Service des Photons, Atomes et Molécules,  
Centre d'Etudes de Saclay, 91191 Gif-sur-Yvette Cedex, France*

(Received 15 July 1994; revised manuscript received 3 October 1994)

The laser-induced multifragmentation of  $C_2H_2$  into protons and multicharged carbon ions is shown to be a direct instantaneous explosion of the molecule. The evolution of the overall nuclear structure is studied through ion-ion correlation peak shapes. The ratios of the maxima of the kinetic-energy release distributions to the Coulomb repulsion energies calculated at the equilibrium internuclear distances are measured to be 45% for the protons and 53% for the  $C^{Z^+}$  ions for all the detected  $H^+ + C^{Z^+} + C^{Z^+} + H^+$  fragmentation channels. The time scale for electronic polarization and stripping compared with the intramolecular electronic and nuclear time evolutions does not allow using a frozen molecular ion structure for the description of the explosion, thus explaining in part the observed fragmentation pattern. During the laser-induced alignment and subsequent stabilization of the molecular frame around the laser polarization direction, the carbon-carbon axis undergoes small damped oscillations that remain larger than the corresponding oscillations of the hydrogen-hydrogen axis. This difference comes from the lower moment of inertia of the hydrogen atoms compared with that of the carbon atoms in the molecule. However, the subsequent deviation from the initial linear structure remains small and is observed when the molecular ion is not completely aligned along the laser electric field.

PACS number(s): 33.80.Rv, 33.80.Eh, 42.50.Vk

### I. INTRODUCTION

The multiple ionization of molecules by different excitation sources is now a subject covering a wide area of activities in atomic and molecular physics. In particular, femtosecond and picosecond lasers are now able to produce electric fields that are no longer small compared to the molecular fields experienced by the valence electrons. Molecular multiphoton multiple ionization has been studied with photon energies in the range 1.17–6.42 eV, corresponding to the available short-pulse duration amplified laser systems [ $Nd^{3+}$ :YAG solid-state to ArF gas laser media (where YAG denotes yttrium aluminum garnet)] [1–10]. The consequence of the electron emission is the dissociative ionization, producing multicharged atomic fragments and showing the characteristic of Coulomb explosion, but with kinetic-energy releases lower than expected from the Coulomb repulsion of pointlike charges. For instance, in the case diatomic molecules  $AB$  composed of light atomic elements such as  $N_2$ , the fragmentation channels  $A^{Z^+} + B^{Z^+}$  exhibit kinetic-energy releases  $E_{\text{expt}} = 0.45ZZ'/R_e$  (a.u.), where  $R_e$  is the equilibrium internuclear distance [11]. Most of the experiments are performed with diatomic molecules in order to determine the specific dynamics of the laser-molecule interaction.

The aim of this experimental work is to study the multifragmentation of polyatomic ions using a Ti:Sa femtosecond laser field at  $\lambda = 790$  nm and in the  $10^{15}$ – $10^{16}$  W/cm<sup>2</sup> intensity range. The first question that arises in short-pulse laser multielectron ionization is whether the multifragmentation results from a sequence of molecular dissociations or from a direct instantaneous explosion. In the case of a sequential multifragmentation, daughter molecular ions are produced from the laser-molecule in-

teraction and can give atomic ions either by unimolecular processes or by a subsequent interaction with the laser field. On the contrary, the direct multifragmentation produces multicharged atomic ions which are ejected simultaneously from the molecular ion. This situation can be of particular interest for studying the stereostructure of polyatomic species and in particular ions that are not well known from infrared spectroscopy [12]. The second important point is to understand the motional dynamics of the nuclear structure in the strong laser field. For diatomic molecules, it was shown that the internuclear axis rotates during the laser pulse duration in order to align with the laser polarization direction. This was interpreted as the result of a torque due to the strong laser-induced polarizability [6–10]. As a consequence, the laser-induced Coulomb explosion angular distributions are maximum for molecular ions that are completely aligned along the laser electric field. In the case of polyatomic molecules or ions, this alignment process can induce additional nuclear structure deformations, in particular because of chemical elements with different moments of inertia. These possible deviations from the initial molecular structure are important to identify in order to determine the nuclear structure just before the explosion.

For a first study of a four-atom molecule, we choose  $C_2H_2$  because acetylene is linear in both the neutral and ionic ground states with a slightly larger C—C bond distance in the ion. In the  $10^{15}$  W/cm<sup>2</sup> laser intensity range, which is necessary for multiple ionization of the molecule,  $C_2H_2^+$  ions are produced following an eight-photon ionization at  $\lambda = 790$  nm at the beginning of the leading edge of the laser pulse. The processes described in this work mainly originate from the molecular-ion population. Because of the similarities of the neutral molecule

and corresponding ion, we do not expect important structural changes from the first ionization step of neutral acetylene. In particular field ionization seems to be the major mode for further electron emission [5,6]. The laser wavelength is no longer the main parameter, which is verified by the similar overall behavior with our picosecond dye laser system operating at  $\lambda=616$  nm. In this case, the  $C_2H_2^+$  ions are formed following a six-photon ionization of acetylene. In this paper, we report the direct multifragmentation of  $C_2H_2^+$  ions into protons and multicharged carbon ions. Comparing our experimental results with synchrotron excitation data in the spectral range of double ionization of  $C_2H_2$ , we do not observe any sequential fragmentation that gives rise to intermediate daughter molecular ions. The nuclear motion analysis shows that the protons are ejected closer to the laser polarization direction than the associated multicharged carbon ions. This observation is attributed to the fact that the laser-induced rotation is faster for the hydrogen atoms than for the carbon atoms in the molecule, thus producing a small deviation from the initial linear structure of the  $C_2H_2^+$  ions when the molecular ion is not thoroughly aligned along the laser polarization direction. This is interpreted in terms of small damped oscillations of the nuclear structure around the laser electric field. The paper is organized as follows. Section II gives the experimental details. Section III presents the major mode of the molecular multifragmentation with the associated Coulomb explosion channels. Section IV describes the dynamics of the nuclear motions in the strong laser field. Finally, Sec. V summarizes the main conclusions of this work.

## II. EXPERIMENT

The laser-induced Coulomb explosion of the molecule is produced by a 130-fs Ti:Sa laser system operating at  $\lambda=790$  nm and focused intensities up to  $2 \times 10^{16}$  W/cm<sup>2</sup> (CEA/DRECAM laser facility). The multicharged atomic and molecular ion species are detected by time-of-flight spectrometry associated with the covariance mapping technique [5,13]. A Wiley-McLaren double-chamber ion spectrometer is operated so that the ion time-of-flight  $T$  is a linear function of the projection of the ion initial momentum  $\mathbf{P}$  along the spectrometer axis  $P_d = P \cos(\theta)$ , where  $P$  is the modulus of  $\mathbf{P}$  and  $\theta$  is the angle between  $\mathbf{P}$  and the ion detection direction [14]

$$T(M, Z, \mathbf{P}) = T(M, Z, \mathbf{P}=0) - P \cos(\theta) / ZeF, \quad (1)$$

where  $e$  is the elementary charge,  $M$  and  $Z$  are, respectively, the mass and charge number of the detected ion, and  $F$  is the collection electric field. The dimensions of the spectrometer (100-mm time-of-flight drift tube, 40-mm apertures, and high transmission grids) are optimized for high collection efficiency and little ion angular discrimination for low collection electric fields ( $F < 200$  V/cm), which give rise to high time-of-flight resolution. In some experiments, the collection electric field  $F$  is increased to ensure 100% collection efficiency in particular for very energetic ions ejected perpendicular to the spec-

trometer axis. The ion signals detected by microchannel plates are recorded with a Lecroy 9450 digital oscilloscope with 2.5 ns per channel temporal resolution and coupled to a personal computer for further statistical analysis. For instance, in Fig. 1, which represents the time-of-flight spectrum of  $C_2H_2$ , each carbon ion  $C^{Z+}$  is represented by two components, due to carbon ions initially ejected toward the detector (forward component  $C^{Z+f}$ ) and in the opposite direction (backward component  $C^{Z+b}$ ). The covariance mapping technique is a statistical method based on correlated fluctuations of ion signals coming from the same fragmentation channels. Figure 2 represents the double ion-ion correlation map of  $C_2H_2$  and the associated time-of-flight spectrum for the  $H^+$ ,  $C^{3+}$ , and  $C^{2+}$  ions. The two-entry correlation coefficient  $R^{(2)}(t_1, t_2)$  appears at  $t_1$  for the horizontal time-of-flight scale and  $t_2$  for the vertical one, when the ions arriving at  $t_1$  and  $t_2$  belong to the same dissociation channel. The correlation coefficient  $R^{(2)}(t_1, t_2)$  is given by

$$R^{(2)}(t_1, t_2) = C^{(2)}(t_1, t_2) / [C^{(2)}(t_1, t_1)C^{(2)}(t_2, t_2)]^{1/2}, \quad (2)$$

where  $C^{(2)}(t_1, t_2) = \langle s(t_1)s(t_2) \rangle - \langle s(t_1) \rangle \langle s(t_2) \rangle$  is the covariance coefficient of the ion signals  $s(t_1)$  and  $s(t_2)$  at times of flight  $t_1$  and  $t_2$ . The brackets  $\langle \rangle$  represent the average values of the ion signals  $s(t_1)$ ,  $s(t_2)$  and the ion signals products  $s(t_1)s(t_2)$  obtained over a great number of laser shots (typically 25 000). The correlation coefficient  $R^{(2)}(t_1, t_2)$  is defined as the covariance coefficient  $C^{(2)}(t_1, t_2)$  normalized by the signal root mean squares  $[C^{(2)}(t_1, t_1)]^{1/2}$  and  $[C^{(2)}(t_2, t_2)]^{1/2}$  at  $t_1$  and  $t_2$  and ranges from  $-1$  for an exact anticorrelation,  $0$  for two independent fluctuations, and  $+1$  for an exact correlation. Due to the microchannel plates' response and spectrometer transmission, the order of magnitude of the measured correlation coefficients is 10% for two different ions belonging to the same fragmentation channel. For instance, islands labeled  $a$ ,  $b$ ,  $c$ , and  $d$  in Fig. 2 represent the correlations of the  $C^{2+b}$  ion with, respectively,  $C^{2+f}$ ,  $C^{3+f}$ ,  $H^+$ , and  $H^+$ . Notice that the  $C^{2+b}$  ion is not correlated with the  $C^{3+b}$  ion, since in  $C_2H_2$  two different carbon ions cannot be ejected in the same direction, i.e.,

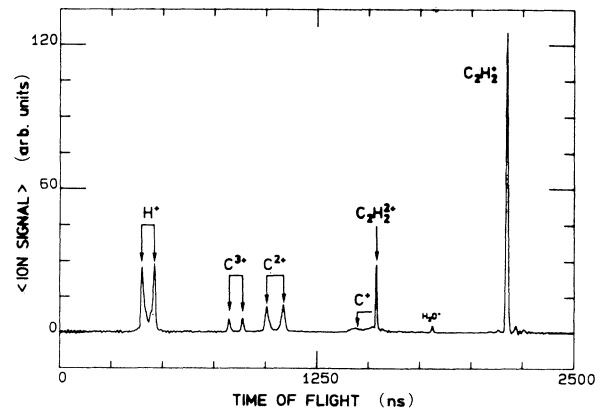


FIG. 1. Ion time-of-flight spectrum of  $C_2H_2$ , obtained at  $\lambda=790$  nm and  $I=2.5 \times 10^{15}$  W/cm<sup>2</sup>.

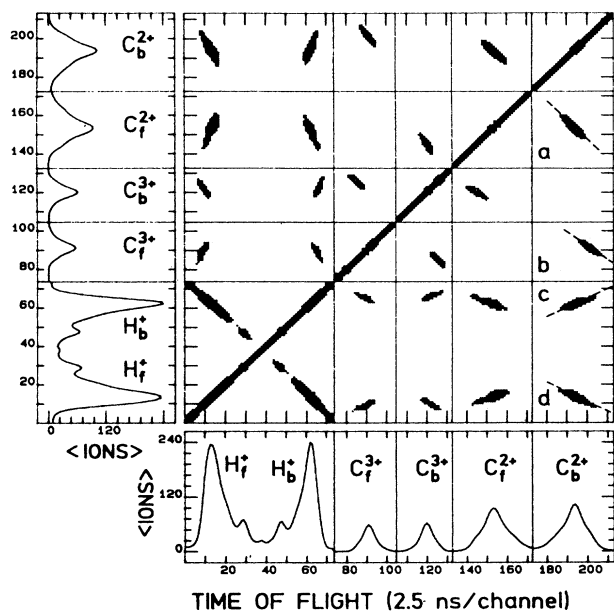


FIG. 2. Double ion-ion correlation map of  $\text{C}_2\text{H}_2$  and associated time-of-flight spectrum for  $\text{H}^+$ ,  $\text{C}^{3+}$ , and  $\text{C}^{2+}$  ions recorded at  $\lambda=790$  nm and  $I=2.5 \times 10^{15}$  W/cm $^2$ . The correlation coefficient  $R^{(2)}$  appears as a dot when it is larger than 5%. Islands *a*, *b*, *c*, and *d* represent the correlation locations of the  $\text{C}_b^{2+}$  ion with  $\text{C}_f^{2+}$ ,  $\text{C}_f^{3+}$ ,  $\text{H}_b^+$ , and  $\text{H}_f^+$ , respectively. The reported lines represent the lines of the maximum correlation coefficients and are analyzed as a function of the  $\text{C}_b^{2+}$  momentum in Fig. 3 with the same labels (a)–(d).

the opposite direction of the detector in this case.

In the case of diatomic molecules  $AB$ , the two-entry double correlation  $R^{(2)}(t_1, t_2)$  is sufficient for the identification of the two-ion channels  $A^{Z+} + B^{Z'++}$ , where  $t_1$  and  $t_2$  represent, respectively, the  $A^{Z+}$  and  $B^{Z'++}$  ion times of flight. For a four-atom molecule such as  $\text{C}_2\text{H}_2$ , double correlations can be used, but with additional criteria, in order to identify four-ion fragmentation channels  $\text{H}^+ + \text{C}^{Z'++} + \text{C}^{Z+} + \text{H}^+$ . Let us make an example with the  $\text{C}_b^{2+}$  ion. For each correlation island in Fig. 2, there is a line of maximum correlations. The resulting correlation coefficients along these lines are plotted in Figs. 3(a)–3(d) as a function of the  $\text{C}_b^{2+}$  initial momentum for islands labeled *a*–*d* in Fig. 2. Figure 3(t) represents the average  $\text{C}_b^{2+}$  total ion count. Finally the abscissa scale for the five curves of Fig. 3 is the same and corresponds to the projection  $P_{\parallel} = P_d$  of the  $\text{C}_b^{2+}$  ion momentum along the spectrometer axis. Figures 3(a) and 3(b) shows that the maxima of the  $\text{C}_f^{2+}/\text{C}_b^{2+}$  and  $\text{C}_f^{3+}/\text{C}_b^{2+}$  correlations occur respectively at 11 and 17 eV for  $\text{C}_b^{2+}$  ions. These different kinetic energies come from the fact that there is more kinetic-energy release in the  $\text{C}^{3+} + \text{C}^{2+}$  channel than in the  $\text{C}^{2+} + \text{C}^{2+}$  channel due to Coulomb repulsion. Figures 3(c) and 3(d) show that the maxima of the  $\text{H}_b^+/\text{C}_b^{2+}$  and  $\text{H}_f^+/\text{C}_b^{2+}$  correlations occur also at 11 and 17 eV for  $\text{C}_b^{2+}$ . As a conclusion, the 11- and 17-eV  $\text{C}_b^{2+}$  ions belong, respec-

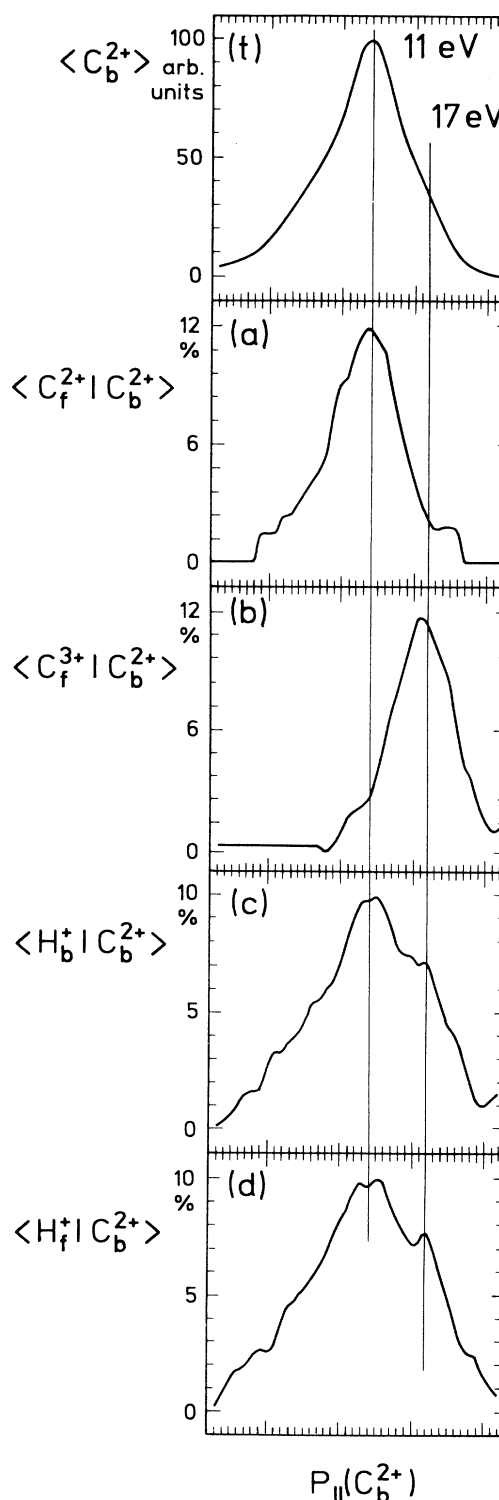


FIG. 3. (t) Momentum spectrum of the  $\text{C}_b^{2+}$  ions. The notation  $\langle \text{C}_b^{2+} \rangle$  stands for the averaged number of the ion count in arbitrary units. (a)–(d) Correlation coefficients along the lines of maximum correlation as a function of the  $\text{C}_b^{2+}$  momentum  $P_{\parallel}$  along the spectrometer axis corresponding to islands *a*–*d* in Fig. 2. The notation  $\langle X^{Z+d} | \text{C}_b^{2+} \rangle$  represents the correlation coefficient of  $\text{C}_b^{2+}$  ions with  $X^{Z+d} = \text{C}^{2+}$ ,  $\text{C}^{3+}$ , or  $\text{H}^+$  ions in the  $d = f$  (forward) or  $b$  (backward) direction.

TABLE I. Fragmentation channels identified from Fig. 2. The ion column represents the ions belonging to the specified fragmentation channel.  $E_{\text{expt}}$  represent the measured kinetic energies at the maximum of the correlated ion energy distributions. The relative accuracy of the measurements is 5%.  $E_{\text{Coul}}$  is the corresponding calculated kinetic energy from the equations of motion for the Coulomb explosion of the molecular ion (see text). Finally, the ratio  $E_{\text{expt}}/E_{\text{Coul}}$  is expressed in percent.

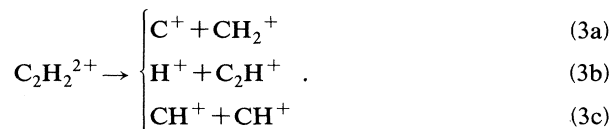
Channel	Ion	$E_{\text{expt}}$ (eV)	$E_{\text{Coul}}$ (eV)	$E_{\text{expt}}/E_{\text{Coul}}$ (%)
$\text{H}^+ + \text{C}^{2+} + \text{C}^{2+} + \text{H}^+$	$\text{H}^+$	18	42.4	42
	$\text{C}^{2+}$	11	20.7	53
	$\text{C}^{2+}$	11	20.7	53
	$\text{H}^+$	18	42.4	42
$\text{H}^+ + \text{C}^{3+} + \text{C}^{2+} + \text{H}^+$	$\text{H}^+$	25	57.5	43
	$\text{C}^{3+}$	16	30.0	53
	$\text{C}^{2+}$	17	31.9	53
	$\text{H}^+$	23	48.8	47
$\text{H}^+ + \text{C}^{3+} + \text{C}^{3+} + \text{H}^+$	$\text{H}^+$	29	64.7	45
	$\text{C}^{3+}$	24	45.9	52
	$\text{C}^{3+}$	24	45.9	52
	$\text{H}^+$	29	64.7	43

tively, to the  $\text{H}_f^+ + \text{C}_f^{2+} + \text{C}_b^{2+} + \text{H}_b^+$  and  $\text{H}_f^+ + \text{C}_f^{3+} + \text{C}_b^{2+} + \text{H}_b^+$  channels. In order to know the kinetic-energy releases of the associated ions, we analyze in the same way the correlation coefficients as a function of these ion initial momenta. The identification of the  $\text{C}_2\text{H}_2$  fragmentation channels from Fig. 3 is summarized in Table I, where the measured kinetic-energy releases are reported for each ion species. The overall relative accuracy of the measurements is estimated to be 5%.

### III. COULOMB EXPLOSION FRAGMENTATION CHANNELS

The ion time-of-flight spectrum presented in Fig. 1 exhibits only two molecular components  $\text{C}_2\text{H}_2^+$  and  $\text{C}_2\text{H}_2^{2+}$ . The absence, or the very weak contribution to the total ion signal, of molecular ion species such as  $\text{C}_2\text{H}^+$ ,  $\text{CH}^+$ , and  $\text{CH}_2^+$  means that the fragmentation channels involving these ions are not produced during the laser interaction. One might think of a complete fragmentation due to the high laser field. This is not the case because of the spatial distribution of the focused laser intensity. Molecular ions that would be completely dissociated at the spatial hottest point of the laser are nevertheless detected because they come from outer regions where the laser intensity is significantly lower. This is the reason why  $\text{C}_2\text{H}_2^+$  and  $\text{C}_2\text{H}_2^{2+}$  ion peaks appear in time-of-flight spectrum. Therefore, the strong atomic  $\text{H}^+$  and  $\text{C}^{Z+}$  ( $Z=1,2,3$ ) ion peaks correlated to the weakness of the above intermediate molecular ion peaks are a signature for a direct instantaneous explosion of the

$\text{C}_2\text{H}_2^+$  ion after the removal of the electrons by the strong laser field. For instance, in comparison with synchrotron excitation in the spectral range of double ionization, one could expect the following channels producing molecular ions [15]:



In particular, the branching ratio for channel (3b) is measured to be 57%, so that we could expect a noticeable  $\text{C}_2\text{H}^+$  ion contribution in the time-of-flight spectrum. The laser excitation results and the comparison with synchrotron excitation show that the molecular spectrum does not play a significant role in the laser-molecular ion coupling. In particular, the dissociative states detected and identified in the synchrotron experiment are not populated in the laser excitation. Molecular bonds do exist during the multiple electron ionization that gives rise to the molecular explosion.

In order to analyze in more detail the Coulomb explosion pattern, one has to consider the results coming from the correlation technique (Figs. 2 and 3), which are summarized in Table I. Previous experiments on diatomic molecules have shown that the kinetic energies measured at the maxima of the ion energy distributions are independent of the laser intensity, pulse durations in the picosecond and femtosecond regimes, and even the laser wavelengths [3,5]. The same behavior is observed in this work with our dye laser system at 616 nm and 2 ps pulse duration and the Ti:Sa laser at 790 nm and 130 fs pulse duration. The main Coulomb explosion observed channels are  $\text{H}^+ + \text{C}^{Z'+} + \text{C}^{Z''+} + \text{H}^+$  with  $|Z' - Z| = -1, 0, 1$ . This situation is similar to that for diatomic molecules and is called charge-symmetric fragmentation [5]. For the same number of missing electrons of the transient molecular ion, the successive ionization potentials associated with the  $|Z' - Z| = -1, 0, 1$  charge states are smaller than those associated with larger  $|Z' - Z|$ . Thus the multielectron ionizations occurs at the lowest thresholds, i.e., for charge-symmetric channels. In Table I we report the calculated Coulomb energies for each ion belonging to a specified pathway. The initial conditions of the explosion are pointlike charges at rest and separated by the  $\text{C}_2\text{H}_2^+$  molecular ion internuclear distances calculated by Lee, Rice, and Schaeffer with the multiconfiguration self-consistent field method:  $R_e(\text{C}-\text{H}) = 1.096 \text{ \AA}$  and  $R_e(\text{C}-\text{C}) = 1.273 \text{ \AA}$  in the linear configuration [16]. The coupled equations of motion are solved by using pure Coulomb repulsive potentials and the final momenta and kinetic energies are obtained for each ion. For this calculation, the molecular frame is aligned along the laser polarization direction before the explosion. This statement is correct for a comparison with energies measured at the maxima of the ion distribution. Small deviations for molecules that are not completely aligned will be analyzed in Sec. IV. The second point of the initial conditions concerns the particles at rest. Although vibrational internal energy should be present at the beginning of the explo-

sion, in particular, due to the alignment process, it remains small compared to the Coulomb repulsion energies of several tens of electron volts. The initial momenta can be neglected in this classical mechanics first approximation. The most striking feature that appears in Table I is that we get the same ratios  $E_{\text{expt}}/E_{\text{Coul}}=52\%$  or  $53\%$  for the  $C^{Z+}$  ions, whatever channel they come from. For the protons, the same behavior is observed with a value around  $45\%$ . These measurements are consistent with previous measurements on diatomic molecules, where it was found that the ratio  $E_{\text{expt}}/E_{\text{Coul}}$  remains constant. The first hypothesis is to assume a simple Coulomb repulsion of the atomic ions following the electrons ejection. In this case, the Coulomb explosion occurs at internuclear distances larger than the molecular ion equilibrium distances. In addition, since the ratio  $E_{\text{expt}}/E_{\text{Coul}}$  remains constant, we do not expect a noticeable increase of the internuclear distances during the electron stripping from one channel to a higher charge state channel, for instance, for  $H^+ + C^{2+} + C^{2+} + H^+$  to  $H^+ + C^{3+} + C^{3+} + H^+$ . As a consequence of a bare Coulomb repulsion of atomic ions, the experimental results exhibit the Coulomb explosion of a modified molecular ion with fixed larger internuclear distances.

The simplest model of the molecular behavior in the strong laser field is to consider mechanical effects that take place in the molecular ion  $C_2H_2^+$  before the Coulomb explosion. In this two-step approach of the laser-molecule interaction, the first step is the ionization of the neutral molecule and the alignment of the resulting molecular ion along the laser polarization direction as observed for diatomic molecules [6–10]. During the violent orientation and stabilization of the ion along the laser electric field, the bond lengths increase with a stabilization at larger values than the equilibrium distances due to the combined effects of centrifugal forces and molecular binding forces. The second step is the multiple ionization of the modified molecular ion. As a consequence, the resulting Coulomb explosion exhibits the observed properties with lower kinetic-energy releases and constant ratios  $E_{\text{expt}}/E_{\text{Coul}}$  because of the larger dimensions of the exploding molecular ion.

However, in a more elaborate model, one has to consider as a whole the strong coupling of the bound molecular electrons with the strong laser field, which is responsible for polarizability and orientation, dressed electronic states and light-induced vibrational states, and the quiver motion of the electrons freed from the molecule around the molecular ion core in the high laser field. In particular, in the above simple mechanical model, the increase of the internuclear distances is due to the orientation of the molecular ion. Another source of bond lengthening and stabilization can come from bond softening effects in the molecular ions, which were observed by Bucksbaum and co-workers in the case of  $H_2^+$  [17,18]. The molecular ion exhibits dressed states that are coherent superpositions of field-free bonding and antibonding electronic states coupled by the strong laser field. The molecular ionic population can be trapped in light-induced vibrational states at larger internuclear distances because the avoided crossings and the resulting dressed potential wells take place

beyond the field-free equilibrium internuclear distances [18]. In addition to this process, the motion of electrons promoted to the ionization continuum in the strong laser field can modify the fragmentation dynamics through electron-nuclear couplings, before they leave the vicinity of the molecule. Following the ideas of Schafer *et al.* [19] and Corkum [20] developed for a unified theory of optical harmonic generation and above-threshold ionization, the quiver motion of these electrons gives rise to scattering processes from the molecular ion core. The time scale of the electron quiver motion is the laser period  $2.6$  fs at  $790$  nm, which is much longer than the electronic time scale in the molecular field and of the same order of magnitude as nuclear vibration periods. There is time for nuclear evolution during electron-nuclei couplings, which can result from scattering of the quivering electron as it returns to the ion core. These ideas and corresponding calculations are well developed for atomic potentials and remain to be investigated for molecular potentials. In any case, the electrons are not ejected suddenly from their site with a frozen nuclear structure during their departure. We conclude this section with the observation of a direct instantaneous explosion of the  $C_2H_2^+$  ion, but with lower kinetic-energy releases than expected from Coulomb repulsion at the equilibrium internuclear distances. The main cause of this observation is to be found in the time scale of the laser-molecule interaction compared to the molecular electronic and nuclear time scales. The nuclear structure does not remain frozen during the laser-molecule interaction in the processes of orientation, bond softening, and electron scattering from the molecular ion core. A time-dependent quantum-mechanical calculation is required to identify the contribution of the above physical effects in the same lines of the theory developed for atoms in strong laser fields [19,20].

#### IV. LASER-INDUCED NUCLEAR MOTIONS

In the preceding section the direct explosion of the molecule was analyzed with the associated fragmentation channels for an averaged linear structure of the molecular ion. However, Coulomb explosion occurs for molecules that are not completely aligned along the laser polarization direction. Since the experiments are performed over a great number of laser shots and because of the probabilistic nature of the molecular response, the observations represent a distribution of molecular ions that is maximum for linear structure and complete alignment. In this section we show how to get additional information on the resulting nuclear motions from the ion correlation peak shapes. The extensions of the correlation islands are due to ions different initial momenta along the spectrometer axis for a same fragmentation channel. The momentum distribution  $\Delta P_d(A^{Z+})$  for a particular  $A^{Z+}$  ion is related to the time-of-flight distribution  $\Delta T(A^{Z+})$  following Eq. (1):

$$\Delta P_d(A^{Z+}) = Z \Delta T(A^{Z+}). \quad (4)$$

In Fig. 2 the  $C^{Z'+}/C^{Z+}$  correlations take place in elongated shapes of time-of-flight slopes equal to  $-Z/Z'$

or momenta slopes  $-1$ , which means that the carbon ions are ejected with opposite and same modulus initial momenta as for a diatomic molecules due to the symmetry of acetylene. More interesting are the  $H^+/C^{Z+}$  time-of-flight and momenta slopes, respectively,  $\Delta T(H^+)/\Delta T(C^{Z+})$  and  $\Delta P_d(H^+)/\Delta P_d(C^{Z+})$ , along the lines of maximum correlation coefficients. These quantities are summarized in Table II according to the charge state  $Z$  of the carbon ion. They correspond to absolute values for the observed  $H^+_f/C^{Z+_f}$ ,  $H^+_f/C^{Z+_b}$ ,  $H^+_b/C^{Z+_f}$ , and  $H^+_b/C^{Z+_b}$  correlation slopes, which are measured to be nearly identical for the four islands which belong to the same  $H^+/C^{Z+}$  correlation group. The ratio  $\Delta P_d(H^+)/\Delta P_d(C^{Z+})$  does not depend dramatically on the carbon charge state. Finally the four-island pattern of the  $H^+/C^{Z+}$  correlations does not change dramatically when the laser polarization direction is turned with respect to the detection axis.

The simplest model is to consider a distribution of stiff linear molecules around the laser polarization axis, which produces ion momenta along the spectrometer axis  $P_d = P \cos(\theta)$  with the same  $\theta$  angle between the momentum  $\mathbf{P}$  and the detection axis for protons and carbons ions. If the observed variations of  $P_d$  are due to the angular distribution of  $\theta$  around the zero value, then we have

$$\Delta P_d(H^+)/\Delta P_d(C^{Z+}) = P(H^+)/P(C^{Z+}). \quad (5)$$

The moduli of the proton and carbon momenta  $P(H^+)$  and  $P(C^{Z+})$  are available from the experimental data at the maxima of the correlation peaks. Using the above equation, the slopes are calculated to be 0.37, 0.36, and 0.32 for the channels reported in Table II. The disagreement with the experimental values means that there are variations of the measured momenta  $P_d$  along the spectrometer axis in addition to the overall rotation of the molecular frame. Since the stiff molecule model fails to explain the observed slopes, we have to consider the stretching and bending motions during the laser-molecule interaction and the resulting explosion. The predicted stretching vibrational frequencies are 3285, 1812, and 3204  $\text{cm}^{-1}$  in the  $D_{\infty h}$  linear configuration of  $C_2H_2^+$ , while the bending frequencies are significantly lower 741, 505, 710, and 697  $\text{cm}^{-1}$  including the Renner-Teller pair of potential surfaces [16]. As a consequence of the alignment process, bending motions are more likely to occur due to the lower force constants [21]. Following this hypothesis, we can calculate the final momenta for each ion in a more general form with respect to the detection and

polarization directions represented, respectively, by the unit vectors  $\mathbf{e}_d$  and  $\mathbf{e}_p$ . Assuming an initial linear configuration of the ion, the rotation process takes place in a plane, which can be referenced by the angle  $\phi$  with the plane defined by  $\mathbf{e}_p$  and  $\mathbf{e}_d$ . In the rotation plane, the final momenta will have an angle  $\theta$  with the  $\mathbf{e}_p$  laser polarization axis vector. Finally if  $\theta_{pd}$  represents the angle between the  $\mathbf{e}_p$  and  $\mathbf{e}_d$  vectors, the measured momentum along the  $\mathbf{e}_d$  detection axis vector is

$$P_d = P(\theta)[\sin(\theta) \cos(\phi) \sin(\theta_{pd}) + \cos(\theta) \cos(\theta_{pd})]. \quad (6)$$

$P(\theta)$  is the modulus of the momentum  $\mathbf{P}$  and does not depend on the angle  $\phi$  because of the cylindrical symmetry around the laser polarization direction. This formulation is different from that given in Eq. (1) in Sec. II. Here the angles  $\theta$  and  $\phi$  are physical parameters associated with the nuclear motions relative to the laser electric field, while the angle  $\theta_{pd}$  represents an experimental parameter relative to the orientation of the detection axis.

The first approximation is to consider that  $P(\theta)$  does not depend on  $\theta$  since  $\theta$  remains close to zero. When the laser polarization direction is parallel to the drift tube axis, i.e.,  $\mathbf{e}_d = \mathbf{e}_p$ , then we find the detected momentum along the spectrometer axis  $P_d = P \cos(\theta)$  as in Eq. (1). At the beginning of this section we observe that the angle  $\theta$  is not the same for the hydrogen and carbon ions. Assuming small values of  $\theta$  around zero, the momentum slopes are

$$\begin{aligned} \Delta P_d(H^+)/\Delta P_d(C^{Z+}) \\ = [P(H^+)/P(C^{Z+})][\theta^2(H^+)/\theta^2(C^{Z+})]. \quad (7) \end{aligned}$$

In order to simplify the discussion we consider only protons and carbon ions ejected in the same direction, i.e.,  $H^+_f/C^{Z+_f}$  or  $H^+_b/C^{Z+_b}$ . The signs of the slopes  $\Delta P_d(H^+)/\Delta P_d(C^{Z+})$  have to be reversed in the other cases using symmetry considerations. The observed slopes are reproduced for  $\theta(H^+) = 0.77\theta(C^{2+})$  in the case of the  $H^+ + C^{2+} + C^{2+} + H^+$  channel and  $\theta(H^+) = 0.83\theta(C^{2+})$  in the case of the  $H^+ + C^{3+} + C^{3+} + H^+$  channel. Because of the square dependence of the angular part of Eq. (7), ejection angles  $\theta(H^+)$  and  $\theta(C^{2+})$  can have opposite signs. A more complete investigation of the fragmentation is obtained with experiments performed at different angles  $\theta_{pd}$  between the laser polarization and spectrometer axis. The four elongated islands pattern is conserved for  $\theta_{pd} = 20^\circ, 40^\circ, 60^\circ$ . Because of the  $\sin(\theta)$  dependence of  $P_d$  in Eq. (4),  $\theta(H^+)$  and  $\theta(C^{2+})$  must have the same sign to keep the observed linear shapes of the correlation peaks. The resulting main observation is that the final angles of ejection are smaller than for the carbon ions.

Finally, it is possible to give estimates of the relative variations of the angles  $\alpha(H)$  and  $\alpha(C)$  between the laser polarization axis and, respectively, the carbon-carbon axis and the hydrogen-hydrogen axis. The relationship between the small angles  $\alpha(H)$  and  $\alpha(C)$  around the zero value is calculated using Coulomb explosion calculations for a slightly nonlinear molecule and the measured ejection angles of the momenta. For the

TABLE II. Time-of-flight slopes  $\Delta T(H^+)/\Delta T(C^{Z+})$  and momenta slopes  $\Delta P_d(H^+)/\Delta P_d(C^{Z+})$  measured in double correlation experiments for  $C_2H_2$ .

$Z$	$\Delta T(H^+)/\Delta T(C^{Z+})$	$\Delta P_d(H^+)/\Delta P_d(C^{Z+})$
1	0.21	0.21
2	0.45	0.22
3	0.67	0.22

$H^+ + C^{2+} + C^{2+} + H^+$  and  $H^+ + C^{3+} + C^{3+} + H^+$  channels, we find, respectively,  $\alpha(H) = 0.88\alpha(C)$  and  $0.91\alpha(C)$ . Both results are very close for both channels: the explosion takes place with similar initial positions conditions. This result is to be related to the fact that the measured kinetic-energy releases do not show any noticeable internuclear increase from channel to channel. Furthermore, the extensions of the correlation islands are due to a distribution of molecular ions with different initial orientations and structures. For each laser shot, there is a probability for detection of a particular geometry which is maximum for completely aligned molecular ions. Because of the proportionality relation  $\alpha(H) = 0.9\alpha(C)$ , the carbon-carbon and hydrogen-hydrogen axes undergo small damped oscillations around the laser electric field with a slightly larger amplitude for the carbon axis. The hydrogen atoms remain closer to the laser polarization axis than the carbon atoms due to their smaller moment of inertia within the molecular ion:  $I(H) = 3.00 \text{ amu } \text{Å}^2$  and  $I(C) = 4.86 \text{ amu } \text{Å}^2$ . However, in the alignment and subsequent stabilization of the molecular frame around the laser electric field, this essentially inertial deviation from the linear structure remains small due to the stiffness of the molecular ion. This interpretation is based on classical mechanics considerations. A more thorough model has to deal with vibrational wave functions to get the molecular spatial distribution including the strong coupling between the laser-induced rotation and bending and stretching motions in a full quantum calculation. This approach will allow a closer and more quantitative description of the experimental data.

## V. CONCLUSION

In this work, the multifragmentation of  $C_2H_2^+$  ions into protons and multicharged carbon ions is shown to be a direct instantaneous explosion of the molecular ion. The systematically lower kinetic-energy releases then ex-

pected from the ion equilibrium internuclear distances are interpreted in terms of strong laser field polarization of the bound and free molecular electrons, which allows deformation of the nuclear structure before the multiple ionization. Several physical mechanisms can modify the molecular ion nuclear structure such as orientation along the laser electric field, bond softening, laser-induced molecular dressed states, and electron quiver motion with the associated scattering processes from the molecular ion before they leave the vicinity of the ion core. In all these cases, the time scale for electron stripping is large enough for electronic and nuclear structure evolution in the strong laser field. The nuclear motions during the explosion are analyzed through the ion-ion correlation peak shapes. We observe small damped oscillations of the molecular frame around the laser polarization direction that produce a distribution of ion momenta detected in correlation experiments. The hydrogen-hydrogen axis remains closer to the polarization direction than the carbon-carbon axis because of the lower moment of inertia associated with the hydrogens. However, the deviation from a linear structure remains small when the molecule is not completely aligned. The laser-induced Coulomb explosion of polyatomic ion species could become a tool for further stereochemical structure studies using small-scale experiments in comparison with ion-beam experiments, provided that more theoretical knowledge would be available about strong laser field effects.

## ACKNOWLEDGMENTS

We are indebted to Dr. J. C. Mialocq for providing us a run with the DRECAM femtosecond laser facility. We are pleased to acknowledge Dr. P. d'Oliveira and P. Maynadier for operating the laser system and M. Bougeard and E. Caprin for their skilled technical assistance.

- 
- [1] L. J. Frasinski, K. Codling, P. Hatherly, J. Barr, I. N. Ross, and W. T. Toner, *Phys. Rev. Lett.* **58**, 2424 (1987).
  - [2] K. Boyer, T. S. Luk, J. C. Solem, and C. K. Rhodes, *Phys. Rev. A* **39**, 1186 (1989).
  - [3] C. Cornaggia, J. Lavancier, D. Normand, J. Morellec, P. Agostini, J. P. Chambaret, and A. Antonetti, *Phys. Rev. A* **44**, 4499 (1991).
  - [4] W. T. Hill, J. Zhu, D. L. Hatten, Y. Cui, J. Goldhar, and S. Yang, *Phys. Rev. Lett.* **69**, 2646 (1992).
  - [5] K. Codling and L. J. Frasinski, *J. Phys. B* **26**, 783 (1993).
  - [6] P. Dietrich, D. T. Strickland, M. Laberge, and P. B. Corkum, in *Molecules in Laser Fields*, edited by A. D. Bandrauk (Marcel Dekker, New York, 1993), p. 181.
  - [7] P. A. Hatherly, L. J. Frasinski, K. Codling, A. J. Langley, and W. Shaikh, *J. Phys. B* **23**, L291 (1990).
  - [8] D. T. Strickland, Y. Beaudoin, P. Dietrich, and P. B. Corkum, *Phys. Rev. Lett.* **68**, 2755 (1992).
  - [9] D. Normand, L. A. Lompré, and C. Cornaggia, *J. Phys. B* **25**, L497 (1992).
  - [10] P. Dietrich, D. T. Strickland, M. Laberge, and P. B. Corkum, *Phys. Rev. A* **47**, 2305 (1993).
  - [11] C. Cornaggia, D. Normand, and J. Morellec, *J. Phys. B* **25**, L415 (1992).
  - [12] G. Herzberg, *Molecular Spectra and Molecular Structure II, Infrared and Raman Spectra of Polyatomic Molecules* (Van Nostrand, New York, 1945).
  - [13] L. J. Frasinski, K. Codling, and P. A. Hatherly, *Science* **246**, 1029 (1989).
  - [14] W. C. Wiley and I. H. McLaren, *Rev. Sci. Instrum.* **26**, 1150 (1955).
  - [15] R. Thissen, J. Delwiche, J. M. Robbe, D. Duflot, J. P. Flament, and J. H. D. Eland, *J. Chem. Phys.* **99**, 6590 (1993).
  - [16] T. J. Lee, J. E. Rice, and H. F. Schaeffer III, *J. Chem. Phys.* **86**, 3051 (1987).
  - [17] P. H. Bucksbaum, A. Zavriyev, H. G. Muller, and D. W. Schumacher, *Phys. Rev. Lett.* **64**, 1883 (1990).
  - [18] A. Zavriyev, P. H. Bucksbaum, J. Squier, and F. Salin, *Phys. Rev. Lett.* **70**, 1077 (1993).
  - [19] K. J. Schafer, Baorui Yang, L. F. DiMauro, and K. C. Kulander, *Phys. Rev. Lett.* **70**, 1599 (1993), and references therein.
  - [20] P. B. Corkum, *Phys. Rev. Lett.* **71**, 1994 (1993).
  - [21] C. Cornaggia, M. Schmidt, and D. Normand, *J. Phys. B* **27**, L123 (1994).